

Evaporative cooling to a Rydberg crystal close to its ground state

M. Brune¹ and D.J. Papoular²

¹Laboratoire Kastler Brossel, Collège de France, CNRS, ENS-Université PSL, Sorbonne Université, France

²LPTM, UMR 8089 CNRS & Univ. Cergy-Pontoise, France

(Dated: November 26, 2019)

We theoretically show how to obtain a long one-dimensional crystal near its quantum ground state. We rely on an evaporative cooling scheme applicable to many-body systems with non-zero-ranged interactions. Despite the absence of periodic potentials, the final state is a crystal which exhibits long-range spatial order. We describe the scheme thermodynamically, applying the truncated Boltzmann distribution to the collective excitations of the chain, and show that it leads to a novel quasi-equilibrium many-body state. For longer chains, comprising about 1000 atoms, we emphasize the quasi-universality of the evaporation curve. Such exceptionally long 1D crystals are only accessible deep in the quantum regime. We perform our analysis on the example of an initially thermal chain of circular Rydberg atoms confined to a one-dimensional (1D) geometry. Our scheme may be applied to other quantum systems with long-ranged interactions such as polar molecules.

Systems presenting long-ranged interactions exhibit strongly-correlated crystalline phases [1–4]. Among them, quantum crystals are those whose constituents undergo large-amplitude zero-point motion [5]. The collective nature of their excitations leads to spectacular phenomena including the Tkachenko oscillations of a vortex lattice in a superfluid [6, 7], the giant plasticity of helium crystals [8], and supersolidity in ultracold gases presenting interactions beyond the contact limit [9–13].

Up to now, the investigation of 1D quantum crystals has been hindered by the difficulty of obtaining large crystals in this geometry, where thermal and quantum fluctuations both destroy long-range order in macroscopic systems [1]. Nevertheless, crystallization does occur in finite-sized systems [15]. It has been unambiguously observed in the absence of any external periodic potential only in small systems of up to fifty ions [16–19] or ten electrons [20, 21]. The realization of larger 1D crystals requires going deep into the quantum regime. There, thermal fluctuations are suppressed, and long-range order is only limited by quantum fluctuations, which are less stringent [1]. The realization of large 1D crystals will pave the way towards the investigation of 1D quantum crystals, where one may look for e.g. giant plasticity through the tunneling of defects [22, 23].

We focus on one way of obtaining spatial order which relies on strong non-zero-range dipole interactions between Rydberg atoms [24]. Rydberg atoms are ideally suited for quantum information processing [25, 26] and quantum simulation [2, 28]. Nontrivial many-body states [29–31] of up to 50 atoms manipulated with optical tweezers have been prepared through resonant coupling to Rydberg states [32–35]. Rydberg states may be weakly admixed to the atomic ground state [36–38] or resonantly excited [39] so as to study the interplay between anisotropic interactions and disorder or frustration [40]. Quantum gases resonantly coupled to Rydberg states have been predicted to exhibit a quantum phase transition to a Rydberg crystal [41], leading to a univer-

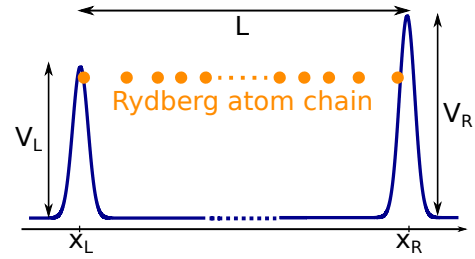


FIG. 1. A Rydberg atom chain (orange) confined in a 1D trap of size L . The potential maxima V_L and V_R satisfy $V_L < V_R$, so that atoms are expelled from the left edge of the trap.

sal scaling behavior observed in the critical region [42].

In all those cases, low-angular-momentum Rydberg states were considered, leading to a strong limitation on the lifetime ($100 \mu\text{s}$ per atom, a few μs for many atoms), limiting the size of the system. Circular Rydberg atoms [43–46], whose excited electron has maximal orbital and magnetic quantum numbers, overcome this limitation and offer a very promising platform for the quantum simulation of many-body problems [2]. Using spontaneous emission inhibition [47, 48], their already long lifetime (30 ms) is expected to be extended to more than 1 min. This timescale allows for implementing an evaporative cooling scheme applicable to Rydberg atoms [2], whose classical analysis shows great promise for reaching extremely low temperatures.

In this Letter, we show that large 1D Rydberg crystals may be prepared very close to their quantum ground state in realistic experimental conditions [2, 49] through this evaporative cooling scheme. Despite the absence of any spatially periodic potential, these crystals exhibit long-range spatial order. This is in stark contrast to the classical analysis of 1D systems, which would predict the absence of long-range order [1]. We introduce a quantum thermodynamic model, applying the truncated Boltzmann distribution to the collective excitations of the chain. We show that it leads to a novel

quasi-equilibrium regime which differs from the truncated Bose–Einstein distribution applicable to quantum-degenerate gases [50]. In contrast to dilute systems where the evaporation is driven by two-body collisions [4], the mechanism we describe here hinges on many-body physics, whereby the phonons present in the chain lead to the expulsion of a single atom. Hence, it is related to the quantum evaporation of liquid helium [52–54], also predicted to affect cold bosonic atoms [55].

We first consider a fixed number N of Rydberg atoms confined in a 1D trap of fixed size L (see Fig. 1). We illustrate our model using the parameters of Ref. [2]. The atoms are confined radially using the ponderomotive potential [56] induced by a Laguerre–Gaussian laser beam [57, chap. 2]. They are trapped axially between two optical plugs yielding the potential $V_T(x) = V_L \exp[-2(x - x_L)^2/w^2] + V_R \exp[-2(x - x_R)^2/w^2]$. The barrier width and heights are, respectively, $w = 30 \mu\text{m}$, $V_L/h = 3 \text{ MHz}$, and $V_R/h = 4 \text{ MHz}$. The trap size $L = x_R - x_L$ is slowly decreased from its initial value so as to induce successive atomic expulsions, providing the evaporative cooling. Unlike for gases, the barrier heights remain constant during the whole process. The atoms interact via the strongly repulsive van der Waals interaction $V(x_i, x_j) = C_6/|x_i - x_j|^6$ with $C_6/h = 3 \text{ GHz } \mu\text{m}^6$, corresponding to ^{87}Rb atoms with the principal quantum number $n = 50$. The equilibrium positions x_1^0, \dots, x_N^0 are evenly spaced in the bulk of the chain, but not on the edges, due to the finite spatial extent of the barriers. Two neighboring atoms are distant by $l \approx 5 \mu\text{m}$, leading to interaction energies $C_6/l^6 \approx h \cdot 200 \text{ kHz}$.

We describe the atomic vibrations in terms of a quadratic Hamiltonian:

$$H = \sum_{k=1}^N \left[\frac{\tilde{p}_k^2}{2m} + \frac{1}{2} m \omega_k^2 \tilde{u}_k^2 \right] \text{ with } \tilde{u}_k = \sum_{n=1}^N R_{nk} u_n. \quad (1)$$

In Eq. (1), the N vibrational modes $\{\tilde{u}_k\}$ have the frequencies $\omega_1 < \dots < \omega_N$, and the $\{\tilde{p}_k\}$ are their conjugate momenta. They are related to the atomic displacements $\{u_n = x_n - x_n^0\}$ through the orthogonal matrix R . The applicability of Eq. (1) only requires local order [58, Sec. I]: the averages $\langle (u_{n+1} - u_n)^2 \rangle^{1/2}$ involving two neighboring atoms should remain small compared to $l = L/N$. For a thermal chain at the temperature T , this requires $k_B T < 2C_6/l^6$, and is well satisfied for up to 1000 atoms with $l \sim 5 \mu\text{m}$ and $k_B T \lesssim h 100 \text{ kHz} \approx k_B 5 \mu\text{K}$.

Classical thermodynamics. For a given configuration characterized by the phonon mode energies $\{\epsilon_k\}_{1 \leq k \leq N}$ and phases $\{\phi_k\}_{1 \leq k \leq N}$, the position of the leftmost atom at time t is $u_1(t) = \sum_k R_{1k} (2\epsilon_k / (m\omega_k^2))^{1/2} \cos(\omega_k t + \phi_k)$. It remains trapped as long as $|u_1(t)| < u_M$, where $u_M = x_1^0 - x_L$. We consider the time-averaged mean-square displacement $\langle u_1^2 \rangle = u_M^2 \sum_{k=1}^N \epsilon_k / E_{Mk}$, where the quantities $E_{Mk} = m\omega_k^2 u_M^2 / R_{1k}^2$ increase with k . Hence, for a given α , the lowest-energy configurations for which

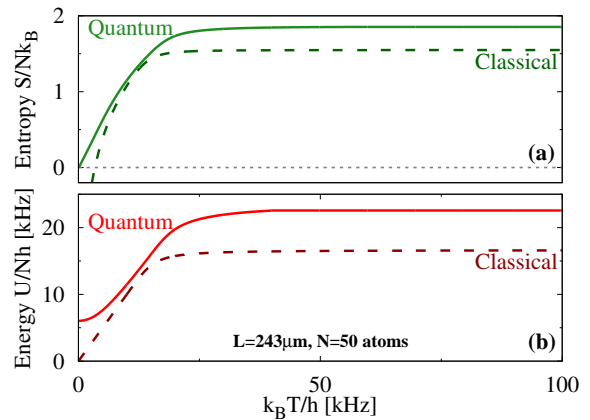


FIG. 2. (a) Entropy and (b) energy per particle for $N = 50$ atoms in a trap of size $L = 243 \mu\text{m}$ (close to the end of the evaporation for the chain of Fig. 4). The solid (dashed) lines show the quantum (classical) prediction.

$\langle u_1^2 \rangle^{1/2} = \alpha u_M$ are those where only the mode $k = 1$ is excited, with the energy $E = \epsilon_1 = \alpha^2 E_{M1}$. For $\alpha = 1/\sqrt{2}$, they correspond to atom 1 barely reaching $u_1 = -u_M$, i.e. to the lowest-energy untrapped configurations. Their energy $E_M^{\text{cl}} = m\omega_1^2 u_M^2 / (2R_{11}^2)$ is set by ω_1 . Furthermore, numerical simulations of the classical (cl) dynamics of the atom chain [59] have shown the atomic motion to be chaotic. Hence, exploiting ergodicity, the trapped configurations are those with $E < E_M^{\text{cl}}$. We describe the quasi-equilibrium thermodynamics of the chain using a Boltzmann distribution truncated at the energy E_M^{cl} , whose partition function reads:

$$Z^{\text{cl}} = \int_{E < E_M^{\text{cl}}} \frac{\prod [d\tilde{p}_k d\tilde{u}_k]}{h^N} e^{-\beta E} = \frac{P(N, \beta E_M^{\text{cl}})}{\beta^N \hbar \omega_1 \dots \hbar \omega_N}. \quad (2)$$

In Eq. (2), $\beta = 1/(k_B T)$ is the inverse temperature, $E = H(\{\tilde{p}_k, \tilde{u}_k\})$ and $P(a, z) = \gamma(a, z)/\Gamma(N)$ is the normalized lower incomplete gamma function [3]. The mean (quadratic) energy $U^{\text{cl}}(L, T)$ associated with the Hamiltonian H and the entropy $S^{\text{cl}}(L, T)$ follow from $U^{\text{cl}} = -\partial \log Z^{\text{cl}}$ and $S^{\text{cl}}/k_B = \log Z^{\text{cl}} - \beta \partial_\beta \log Z^{\text{cl}}$.

The function $P(a, z)$ also appears in the thermodynamics of the evaporation of a gas ($a = 3$ for a harmonic trap) [4]. Here, $a = N$ ranges from 40 to 1000, so that the role of truncation is strongly enhanced with respect to gases of ground-state atoms [58, Sec. III]. It is important for $k_B T \gtrsim E_M^{\text{cl}}/N$. For larger T , all trapped configurations are equally populated. The probability density for a configuration to have the energy E is $NE^{N-1}/(E_M^{\text{cl}})^N$, hence, nearly all configurations have energies $\sim E_M^{\text{cl}}$. Both U^{cl} and S^{cl} reach finite maxima $U_{\text{max}}^N(L)$ and $S_{\text{max}}^N(L)$ (see Fig. 2), where:

$$U_{\text{max}}^{(N)} = \frac{NE_M^{\text{cl}}}{N+1} \text{ and } S_{\text{max}}^{(N)} = k_B \log \left(\frac{(E_M^{\text{cl}})^N / N!}{\hbar \omega_1 \dots \hbar \omega_N} \right). \quad (3)$$

For fixed N , both maxima increase with L , because less

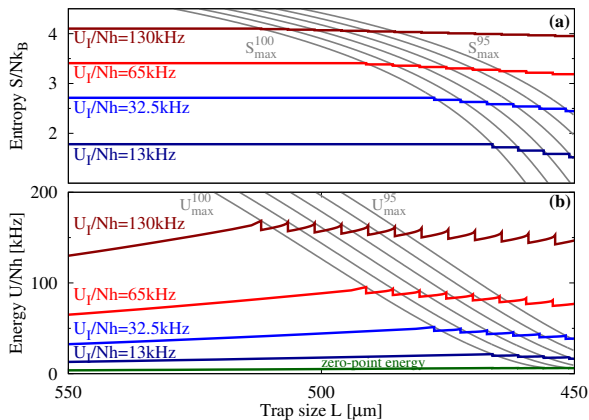


FIG. 3. The first few expulsions for a chain with $N_I = 100$ atoms and $L_I = 550 \mu\text{m}$, in terms of (a) entropy S/N and (b) energy U/N per particle, for various initial energies. The maxima $S_{\text{max}}^{(N)}(L)/N$ and $U_{\text{max}}^{(N)}(L)/N$ are shown in gray. Each expulsion yields a discontinuity in both S and U .

stringent traps will accommodate higher-energy excitations. This novel regime is inaccessible with gases, where an atom whose energy is close to the evaporation threshold is expelled when it undergoes a collision [4, 61]. However, it is accessible for a Rydberg chain [58, Sec. II].

Quantum thermodynamics. For lower quadratic energies, we use a quantum (quant) description. Assuming ergodicity in the quantum regime, we introduce the energy $E_{\mathbf{n}} = \sum_{k=1}^N \hbar\omega_k(n_k + 1/2)$ of the configuration labeled by the integer multiplet $\mathbf{n} = \{n_k\}_{1 \leq k \leq N}$. The threshold energy E_M^{quant} for trapped configurations satisfies:

$$E_M^{\text{quant}} = \min_{\mathbf{n}} \left[E_{\mathbf{n}} \text{ with } \sum_{k=1}^N \frac{\hbar\omega_k(n_k + 1/2)}{E_{Mk}} \geq \alpha^2 \right], \quad (4)$$

where we choose $\alpha = 1/\sqrt{2}$ as in the classical case. The energy E_M^{quant} exceeds both E_M^{cl} and the zero-point energy $E_{\text{ZP}} = \sum_{k=1}^N \hbar\omega_k/2$. The quantum partition function reads $Z^{\text{quant}} = \sum_{\mathbf{n}} e^{-\beta E_{\mathbf{n}}} \Theta(E_M^{\text{quant}} - E_{\mathbf{n}})$, where Θ is the Heaviside function, illustrating an important difference with respect to gases of ground-state atoms. There, the truncation selects the trapped single-particle modes without constraining their populations, yielding a truncated Bose-Einstein distribution [50]. Instead, for Rydberg chains, the truncation involves the configuration energies $E_{\mathbf{n}}$. This prevents Z^{quant} from factorizing and reflects the correlations between the trapped phonon modes, leading to a novel quasi-equilibrium state which does not obey a truncated Bose-Einstein distribution.

We assume $E_M^{\text{quant}} \gg E_{\text{ZP}} + \hbar\omega_N$, which is well satisfied for all parameters considered in this paper. Then, $E_M^{\text{quant}} \approx E_M^{\text{cl}} + E_{\text{ZP}}$. For $k_B T \gtrsim E_M^{\text{quant}}/N$, we evaluate the quantum energy $U^{\text{quant}}(L, T)$ and entropy $S^{\text{quant}}(L, T)$ [58, Sec. III] starting from Eq. (2), replacing E_M^{cl} by E_M^{quant} and including the leading quantum correction, proportional to \hbar^2 [5, §33]. For $k_B T < E_M^{\text{quant}}/N$,

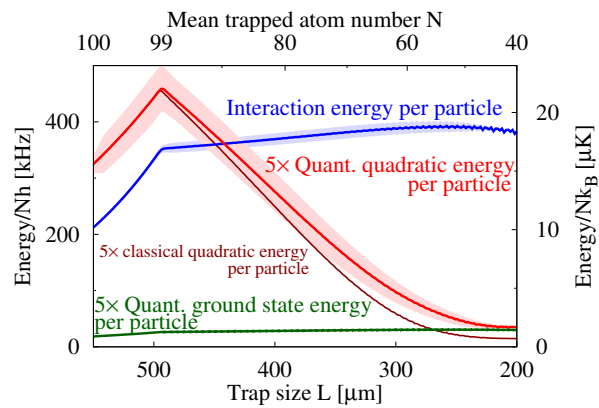


FIG. 4. Classical (dark red) and quantum (red) predictions for the mean quadratic energy, interaction (blue) and ground state (green) energies per particle during the evaporation, starting from $N_I = 100$, $L_I = 550 \mu\text{m}$, down to $N_F = 40$, $L_F = 200 \mu\text{m}$. The shaded red and blue areas show the standard deviations on the quadratic and interaction energies. Energies are measured in kHz, with $h \cdot 100 \text{ kHz} \sim k_B \cdot 5 \mu\text{K}$.

the energy and entropy reflect the non-truncated thermodynamics of a harmonic oscillator chain. They overlap with U^{quant} , S^{quant} for a range of values of T , yielding the full quantum thermodynamic functions (see Fig. 2).

Evaporation. We now describe the evaporation process. Initially, the chain comprises $N = N_I$ atoms in a trap of size $L^{(N)} = L_I$, with the energy $U^{(N)} = U_I$. For all considered parameters, $U_I \gg E_{\text{ZP}}$, signalling the classical regime, and $U_I \ll E_M^{\text{cl}}$, so that it is described by non-truncated thermodynamics. Thus, $U_I/N_I = k_B T_I$ is the initial temperature. We adiabatically compress the chain by slowly decreasing L (see Fig. 3). Hence, the entropy $S^{(N)}$ remains constant. Expelling an atom is irreversible, therefore N also remains constant. However, T and $U^{(N)}$ increase, whereas $U_{\text{max}}^{(N)}(L)$ and $S_{\text{max}}^{(N)}(L)$ decrease. The compression proceeds until the trap no longer accommodates the entropy, i.e. up to the trap size $L_f^{(N)}$ such that $S_{\text{max}}^{(N)}(L_f^{(N)}) = S^{(N)}$. This implies $T \rightarrow \infty$, hence, $U_f^{(N)} = U_{\text{max}}^{(N)}(L_f^{(N)})$. At this point, the leftmost atom is expelled from the trap, its kinetic energy being the barrier height V_L . The $(N-1)$ remaining atoms thermalize to the new initial energy $U_i^{(N-1)}$, where:

$$U_i^{(N-1)} = U_f^{(N)} + V_0^{(N)} - V_0^{(N-1)} - V_L. \quad (5)$$

Here, $V_0^{(N)}$ and $V_0^{(N-1)}$ are the static equilibrium energies for N and $(N-1)$ atoms in a trap of size $L_f^{(N)}$. Then, adiabatic compression resumes until the next expulsion.

The complete evaporation curve consists of a repeated sequence of these two steps. Figure 4 compares our classical (dark red) and quantum (red) predictions, down to the trap size $L_F = 200 \mu\text{m}$ where $E_M^{\text{quant}} \gtrsim E_{\text{ZP}} + \hbar\omega_N$. The result of our classical model closely matches the classical-dynamics simulations reported in Ref. [2]

(Fig. 14, phase II). Our quantum approach predicts that, starting from $N_I = 100$ atoms, the final state with $N_F = 40$ atoms obeys a Bose–Einstein distribution with $U_F/(N_F h) = 7.0$ kHz, slightly above the zero–point energy $E_{ZP}/(N_F h) = 5.9$ kHz. The shown average energies account for the uncertainty $\Delta U_I = U_I/\sqrt{N_I} = h \cdot 6.5$ kHz on U_I , which washes out their jaggedness due to the expulsions (Fig. 3) [58, Sec. IV]. The final state is in the 1D regime if the radial confinement frequency $\omega_\perp/(2\pi) \gg U_F/(N_F h)$. Smaller values of ω_\perp will lead to quasi–1D chains exhibiting the ‘zigzag’ transition observed with ion chains [23, 63] and in electronic systems [64].

Quasi–universality for longer chains. Finally, we focus on long chains with $N_I \approx 1000$, keeping $l_I = L_I/N_I = 5.5 \mu\text{m}$. Then, the inhomogeneities near the trap edges are negligible, and both $S/N = s(l, T)$ and $U/N = u(l, T)$ only depend on $l = L/N$ and T . The evaporation is conveniently described in terms of l , s , u , and the atom number fraction $n = N/N_I$. The evaporation curve consists of two parts (see Fig. 5). First, the initial compression at constant N_I depends on $u_I = U_I/N_I$. The second part consists of all subsequent expulsions and compressions. The mean distance l increases at each expansion and decreases during each compression; on average, l decreases. The quantities s and u always remain close to the universal curves $s_{\text{max}}(l) = S_{\text{max}}(N, L)/N$ and $u_{\text{max}}(l) = U_{\text{max}}(N, L)/N$, respectively [58, Sec. V]. Their fluctuations, visible in the insets of Fig. 5 for $N_I = 1000$ and $k_B T_I/h = 65$ kHz, decrease with increasing N_I for two reasons. First, the changes δu and δs in the energy and entropy per particle upon expelling an atom are decreasing functions of N . Second, larger N_I lead to smaller $\Delta U_I = U_I/\sqrt{N_I}$ and, hence, to smaller uncertainties on s and u . Quasi–universality also applies to the fluctuations Δu and Δs on the energy and entropy [58, Sec. V].

The fraction $n = N/N_I$ (Fig. 5(c)) is not universal [58, Fig. S6]. For $N_I = 1000$, n reaches a stationary value n_F as u goes to $e_{ZP}(l) = E_{ZP}(l)/N$. The value $n_F(u_I)$ is a decreasing function of $u_I = U_I/N_I$. The curves on Fig. 5 are truncated at the minimum value $l = 4.4 \mu\text{m}$ where $E_M^{\text{quant}} \gtrsim E_{ZP} + \hbar\omega_N$. Then, for $k_B T_I/h = 65$ kHz, the chain comprises $N_F = 764$ atoms with the energy $U_F/(N_F h) = 8.5$ kHz, close to $E_{ZP}/(N_F h) = 6.6$ kHz.

The final state of such a long chain is a crystal exhibiting true long–range order, with all spatial correlators $C_{nm} = \langle (u_n - u_m)^2 \rangle \ll l^2$ [58, Fig. S1]. This is only possible deep in the quantum regime, where thermal fluctuations are suppressed [1]. The crystalline order may be fully characterized experimentally through microwave spectroscopy, revealing the regularity and fluctuations of the lattice parameter, combined with spatially–resolved ground state imaging [33, 65].

We have introduced a quantum thermodynamic model for the evaporative cooling of 1D Rydberg atom chains [2]. Unlike the evaporative cooling of ground–state atoms, the final temperatures accessible with our scheme

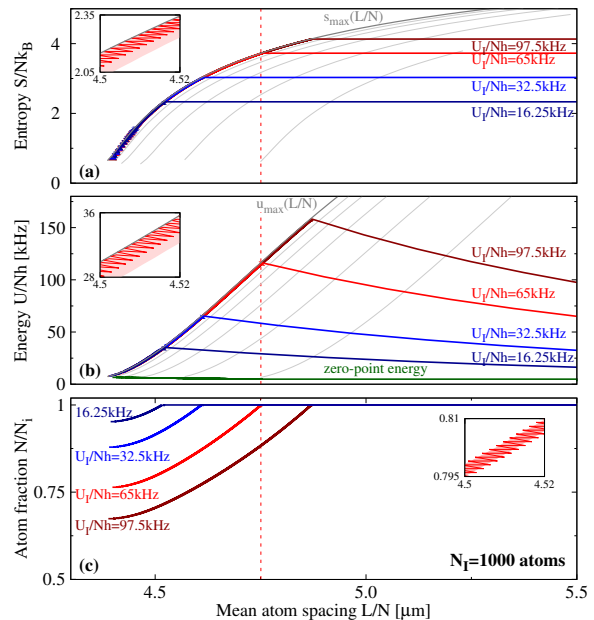


FIG. 5. Quasi–universal evaporation of a chain with $N_I = 1000$ and $l_I = 5.5 \mu\text{m}$, in terms of the mean (a) entropy and (b) energy per particle, for various initial energies. The thin gray lines show $S_{\text{max}}(L/N)/N$ and $U_{\text{max}}(L/N)/N$ for $N = 50, 100, 200, 400,$ and 800 (from right to left) which converge towards $s_{\text{max}}(l)$ and $u_{\text{max}}(l)$ (thick gray lines). Panel (c): non–universal atom fraction N/N_I . The vertical red inset shows the first expulsion for $U_I/(N_I h) = 65$ kHz. The insets show in on the same small fraction of the curves for $U_I/(N_I h) = 65$ kHz, and show the jagged curves obtained before averaging; the shaded areas show the standard deviations.

are not of the order of the barrier heights. Instead, they are determined by the maximum energy $u_{\text{max}}(l)$ compatible with the trap. This reflects the many–body character of the evaporation scheme and leads to final temperatures that are radically lower than the barrier heights by three orders of magnitude. We have shown that, under realistic experimental conditions, this scheme yields large near–ground–state Rydberg crystal. The long–range spatial order of these 1D structures is a feature of the deep quantum regime. Our scheme will also apply to other interacting 1D systems such as polar molecules [66, 67]. There, the nonzero–ranged interaction between the particles is provided by the dipole–dipole interaction, which scales with $1/r^3$ and may be made purely repulsive in low–dimensional geometries [68].

Outlook. The following directions warrant further investigation. (i) For higher initial temperatures or mean atom spacings, the initial state is a liquid and Eq. (1) does not hold, but our scheme will still drive the system towards its crystalline ground state. (ii) For longer chains, a prolonged evaporation going beyond the regime of Fig. 5 leads to $E_M^{\text{quant}} \lesssim E_{ZP} + \hbar\omega_N$, in which case the calculation of the quantum thermodynamic functions is more involved. (iii) The timescale ensuring adiabaticity

is set by the anharmonic processes neglected in Eq. (1).
(iv) Our scheme is also applicable in 2D, where the expected ground state is a hexagonal crystal which we shall investigate both theoretically and experimentally.

We acknowledge stimulating discussions with J.M. Raimond, Ph. Lecheminant, Y. Castin, T. Huillet, L.P. Pitaevskii, C. Sayrin, and G.V. Shlyapnikov.

-
- [1] E. Wigner, Phys. Rev. **46**, 1002 (1934).
 [2] C. C. Grimes and G. Adams, Phys. Rev. Lett. **42**, 795 (1979).
 [3] J. G. Bohnet, B. C. Sawyer, J. W. Britton, M. L. Wall, A. M. Rey, M. Foss-Feig, and J. J. Bollinger, Science **352**, 1297 (2016).
 [4] E. Jordan, K. A. Gilmore, A. Shankar, A. Safavi-Naini, J. G. Bohnet, M. J. Holland, and J. J. Bollinger, Phys. Rev. Lett. **122**, 053603 (2019).
 [5] R. A. Guyer, Solid State Physics **23**, 412 (1969).
 [6] E. B. Sonin, Rev. Mod. Phys. **59**, 87 (1987).
 [7] I. Coddington, P. Engels, V. Schweikhard, and E. A. Cornell, Phys. Rev. Lett. **91**, 100402 (2003).
 [8] A. Haziot, X. Rojas, A. D. Fefferman, J. R. Beamish, and S. Balibar, Phys. Rev. Lett. **110**, 035301 (2013).
 [9] J. Li, J. Lee, W. Huang, S. Burchevsky, B. Shteynas, F. C. Top, A. O. Jamison, and W. Ketterle, Nature **543**, 91 (2017).
 [10] J. Léonard, A. Morales, P. Zupancic, T. Esslinger, and T. Donner, Nature **543**, 87 (2017).
 [11] L. Tanzi, E. Lucioni, F. Famà, J. Catani, A. Fioretti, C. Gabbanini, R. N. Bisset, L. Santos, and G. Modugno, Phys. Rev. Lett. **122**, 130405 (2019).
 [12] F. Böttcher, J. N. Schmidt, M. Wenzel, J. Hertkorn, M. Guo, T. Langen, and T. Pfau, Phys. Rev. X **9**, 011051 (2019).
 [13] L. Chomaz, D. Petter, P. Ilzhöfer, G. Natale, A. Trautmann, C. Politi, G. Durastante, R. M. W. van Bijnen, A. Patscheider, M. Sohmen, M. J. Mark, and F. Ferlaino, Phys. Rev. X **9**, 021012 (2019).
 [14] N. D. Mermin, Phys. Rev. **176**, 250 (1968).
 [15] D. Vu and S. Das Sarma, “One-dimensional effective Wigner crystal in quantum and classical regimes,” (2018).
 [16] P. Jurcevic, B. P. Lanyon, P. Hauke, C. Hempel, P. Zoller, R. Blatt, and C. F. Roos, Nature **511**, 202 (2014).
 [17] P. Richerme, Z. Gong, A. Lee, C. Senko, J. Smith, M. Foss-Feig, S. Michalakis, A. V. Gorshkov, and C. Monroe, Nature **511**, 198 (2014).
 [18] C. Senko, J. Smith, P. Richerme, A. Lee, W. C. Campbell, and C. Monroe, Science **345**, 430 (430).
 [19] R. Lechner, C. Maier, C. Hempel, P. Jurcevic, B. P. Lanyon, T. Monz, M. Brownnutt, R. Blatt, and C. F. Roos, Phys. Rev. A **93**, 053401 (2016).
 [20] V. V. Deshpande and M. Bockrath, Nature **4**, 314 (2008).
 [21] I. Shapir, A. Hamo, S. Pecker, C. P. Moca, O. Legeza, G. Zarand, and S. Ilani, Science **364**, 870 (2019).
 [22] S. Balibar, J. Beamish, A. Fefferman, A. Haziot, X. Rojas, and F. Souris, C. R. Phys. **17**, 264 (2016).
 [23] H. L. Partner, R. Nigmatullin, T. Burgermeister, J. Keller, K. Pyka, M. B. Plenio, A. Retzker, W. H. Zurek, A. del Campo, and T. E. Mehlstäubler, Physica B **460**, 114 (2015).
 [24] D. Kleppner, M. G. Littman, and M. L. Zimmerman, Sci. Am. **244**, 130 (1981).
 [25] M. Saffman, T. G. Walker, and K. Mølmer, Rev. Mod. Phys. **82**, 2313 (2010).
 [26] Y. Zeng, P. Xu, X. He, Y. Liu, M. Liu, J. Wang, D. J. Papoular, G. V. Shlyapnikov, and M. Zhan, Phys. Rev. Lett. **119**, 160502 (2017).
 [27] T. L. Nguyen, J. M. Raimond, C. Sayrin, R. Cortinas, T. Cantat-Moltrecht, F. Assemat, I. Dotsenko, S. Gleyzes, S. Haroche, G. Roux, T. Jolicoeur, and M. Brune, Phys. Rev. X **8**, 011032 (2018).
 [28] H. Weimer, M. Müller, I. Lesanovsky, P. Zoller, and H. P. Büchler, Nat. Phys. **6**, 382 (2010).
 [29] T. Pohl, E. Demler, and M. D. Lukin, Phys. Rev. Lett. **104**, 043002 (2010).
 [30] P. Schauss, M. Cheneau, M. Endres, T. Fukuhara, S. Hild, A. Omran, T. Pohl, C. Gross, S. Kuhr, and I. Bloch, Nature **491**, 87 (2012).
 [31] P. Schauss, J. Zeiher, T. Fukuhara, S. Hild, M. Cheneau, T. Macri, T. Pohl, I. Bloch, and C. Gross, Science **347**, 1455 (2015).
 [32] H. Bernien, S. Schwartz, A. Keesling, H. Levine, A. Omran, H. Pichler, S. Choi, A. S. Zibrov, M. Endres, M. Greiner, V. Vuletic, and M. D. Lukin, Nature **551**, 579 (2017).
 [33] D. Barredo, V. Lienhard, S. de Léséleuc, T. Lahaye, and A. Browaeys, Nature **561**, 79 (2018).
 [34] H. Labuhn, D. Barredo, S. Ravets, S. de Léséleuc, T. Macri, T. Lahaye, and A. Browaeys, Nature **534**, 667 (2016).
 [35] S. de Léséleuc, V. Lienhard, P. Scholl, D. Barredo, S. Weber, N. Lang, H. P. Büchler, T. Lahaye, and A. Browaeys, Science **365**, 775 (2019).
 [36] G. Pupillo, A. Micheli, M. Boninsegni, I. Lesanovsky, and P. Zoller, Phys. Rev. Lett. **104**, 223002 (2010).
 [37] Y. Jau, A. M. Hankin, T. Keating, I. H. Deutsch, and G. W. Biedermann, Nat. Phys. **12**, 71 (2016).
 [38] J. Zeiher, R. van Bijnen, P. Schauss, S. Hild, J. Choi, T. Pohl, I. Bloch, and C. Gross, Nat. Phys. **12**, 1095 (2016).
 [39] R. Löw, H. Weimer, J. Nipper, J. B. Balewski, B. Butscher, H. P. Büchler, and T. Pfau, J. Phys. B **45**, 113001 (2012).
 [40] A. W. Glaetzle, M. Dalmonte, R. Nath, I. Rouschatzakis, R. Moessner, and P. Zoller, Phys. Rev. X **4**, 041037 (2014).
 [41] H. Weimer, R. Löw, T. Pfau, and H. P. Büchler, Phys. Rev. Lett. **101**, 250601 (2008).
 [42] R. Löw, H. Weimer, U. Krohn, R. Heidemann, V. Bendkowsky, B. Butscher, H. P. Büchler, and T. Pfau, Phys. Rev. A **80**, 033422 (2009).
 [43] R. G. Hulet and D. Kleppner, Phys. Rev. Lett. **51**, 1430 (1983).
 [44] D. A. Anderson, A. Schwarzkopf, R. E. Sapiro, and G. Raithel, Phys. Rev. A **88**, 031401(R) (2013).
 [45] V. Zhelyazkova and S. D. Hogan, Phys. Rev. A **94**, 023415 (2016).
 [46] A. Signoles, E. K. Dietsche, A. Facon, D. Grosso, S. Haroche, J. M. Raimond, M. Brune, and S. Gleyzes, Phys. Rev. Lett. **118**, 253603 (2017).
 [47] D. Kleppner, Phys. Rev. Lett. **47**, 233 (1981).
 [48] R. G. Hulet, E. S. Hilfer, and D. Kleppner, Phys. Rev. Lett. **55**, 2137 (1985).

- [49] R. G. Cortiñas, M. Favier, B. Ravon, P. Méhaignerie, Y. Machu, J. M. Raimond, C. Sayrin, and M. Brune, arXiv:1911.02316 (2019).
- [50] M. Yamashita, M. Koashi, and N. Imoto, Phys. Rev. A **59**, 2243 (1999).
- [4] O. J. Luiten, M. W. Reynolds, and J. T. M. Walraven, Phys. Rev. A **53**, 381 (1996).
- [52] W. D. Johnston Jr. and J. G. King, Phys. Rev. Lett. **16**, 1191 (1966).
- [53] P. W. Anderson, Phys. Lett. **29A**, 563 (1968).
- [54] F. Dalfovo, A. Fracchetti, A. Latri, L. Pitaevskii, and S. Stringari, Phys. Rev. Lett. **75**, 2510 (1995).
- [55] D. J. Papoular, L. P. Pitaevskii, and S. Stringari, Phys. Rev. A **94**, 023622 (2016).
- [56] S. K. Dutta, J. R. Guest, D. Feldbaum, A. Walz-Flannigan, and G. Raithel, Phys. Rev. Lett. **85**, 5551 (2000).
- [57] L. Allen, S. M. Barnett, and M. J. Padgett, *Optical angular momentum* (Institute of Physics Publishing, 2003).
- [58] M. Brune and D. J. Papoular, “See supplemental material at [url will be inserted by publisher].” (2019).
- [59] M. Brune and J. M. Raimond, “Numerical simulations of the classical dynamics of a trapped Rydberg chain,” (2017), private communication.
- [3] DLMF, “*NIST Digital Library of Mathematical Functions*,” <http://dlmf.nist.gov/> (2018).
- [61] J. T. M. Walraven, in *Quantum dynamics of simple systems* (IOP Bristol, 1996).
- [5] L. D. Landau and E. M. Lifshitz, *Statistical Physics, part 1*, 3rd ed. (Elsevier, 1980).
- [63] G. Birkl, S. Kassner, and H. Walther, Nature **357**, 310 (1992).
- [64] H. Ikegami, H. Akimoto, D. G. Rees, and K. Kono, Phys. Rev. Lett. **109**, 236802 (2012).
- [65] D. Barredo, S. de Léséleuc, V. Lienhard, T. Lahaye, and A. Browaeys, Science **354**, 1021 (2016).
- [66] L. De Marco, G. Valtolina, K. Matsuda, W. G. Tobias, J. P. Covey, and J. Ye, Science **363**, 853 (2019).
- [67] L. Anderegg, L. W. Cheuk, Y. Bao, S. Burchesky, W. Ketterle, K. Ni, and J. M. Doyle, Science **365**, 1156 (2019).
- [68] M. A. Baranov, M. Dalmonte, G. Pupillo, and P. Zoller, Chem. Rev. **112**, 5012 (2012).

Supplemental material

This document provides complementary information on the following topics: I. the applicability of the quadratic Hamiltonian; II. the anharmonic terms and their twofold role; III. the partition function and its numerical evaluation; IV. the observability of the adiabatic plateaux with constant atom numbers; V. the quasi-universal description for long chains and its limits.

THE QUADRATIC HAMILTONIAN

The Hamiltonian describing the harmonic vibrations of the atoms about their equilibrium positions $\{x_n^0\}$ (Eq. 1 in the main text) is applicable as soon as the chain exhibits local order. Indeed, in the chain bulk, the trapping potential is negligible and, within the nearest-neighbor approximation, the interaction energy of atom n is $E_n^I = C_6[1/(x_n - x_{n-1})^6 + 1/(x_n - x_{n+1})^6]$. Here, $x_n = x_n^0 + u_n$ is the position of atom n . Expanding E_n^I to second order in the displacements $\{u_n\}$, and exploiting the near-translational invariance, we find that the harmonic approximation is valid if $\eta_n = 21 \langle (u_{n+1} - u_n)^2 \rangle / l^2 < 1$, where $l = L/N$ is the mean interatomic distance and the average $\langle (u_{n+1} - u_n)^2 \rangle$ is the spatial correlator between two neighboring atoms. For a thermal distribution, this condition reduces to $k_B T < 2C_6/l^6$. Accounting for the trap and the truncated thermodynamics, we find this criterion to be well satisfied all along the evaporation for the long chain of Fig. 5 in the main text (see Fig. S1(a)).

The present criterion is less stringent than asking for the chain to be in a crystalline phase. This is especially true in 1D where thermal fluctuations quickly rule out long-range order [S1]. For example, the long chain of Fig. 5 exhibits no long-range spatial correlations in its initial state ($N_i = 1000$, $l_i = 5.5 \mu\text{m}$, $k_B T_i/h = 65 \text{ kHz}$). This can be seen on Fig. S1(b): the correlator $\langle (u_n - u_m)^2 \rangle / l^2 > 1$ for distant atoms. However, our scheme brings the chain close to its quantum ground state, which does exhibit long-range correlations ($\langle (u_n - u_m)^2 \rangle / l^2 \ll 1$ for all n and m , see Fig. S1(c)).

ANHARMONIC EFFECTS

The leading anharmonic contribution to the Hamiltonian follow from the third- and fourth-order terms in the displacements $\{u_n\}$. For gases, they yield two-body collisions which are essentially instantaneous. By contrast, for Rydberg chains, they generate many-body correlations over the characteristic time τ_{propag} for propagation along the chain, set by the sound velocity. They are mostly due to interactions and occur in the chain bulk, where their probability does not depend on position (see Fig. S2). They are much less probable near the edges,

where the trapping potential leads to larger distances between the static equilibrium positions of the atoms.

The role of these anharmonic processes is twofold. First, they are responsible for thermalization and ergodicity on a timescale involving τ_{propag} . Second, they set the (longer) timescale ensuring the adiabaticity of the compression between two atomic expulsions. The classical-dynamics simulations reported in Ref. [S2] have shown that, for the shorter chain of Fig. 3 in the main text ($N_i = 100$), compression rates of the order of $40 \mu\text{m/ms}$ are adequate. The optimal compression rate will be investigated elsewhere.

For gases, anharmonic processes directly drive the atomic expulsions, which immediately follow two-atom collisions during which one atom has acquired enough energy. Their relation to expulsions is more involved for Rydberg chains. If the trap size is such that an expulsion is expected ($T \rightarrow \infty$), ergodicity causes the system to explore various configurations until the leftmost atom is expelled with the energy V_L . If no expulsion is expected (T finite), the compression of the trap causes an increase in energy due to the atoms on the edges of the chain being set in motion towards the bulk. Expelling the leftmost atom before thermalization has taken place (i.e. with an energy $> V_L$) is likely to involve a two-atom collision at the open end of the trap. There, anharmonic terms are strongly suppressed (see Fig. S2), so that these higher-energy expulsions are rare. Instead, the energy increase is most often mediated, through harmonic vibrations, to the chain bulk where thermalization occurs. The rare cases in which the leftmost atom is expelled are not captured by our thermodynamic model. However, they are not a hindrance as long as their rate remains small: instead, they speed up the evaporation process with respect to our thermodynamic prediction. The presence of a single open end (the left end on Fig. 1 of the main text) is favorable for two reasons: (i) it leads to longer propagation times and, hence, more efficient thermalization; (ii) it helps reduce the rate of non-thermalized expulsions.

THE PARTITION FUNCTION

Normalized lower incomplete Gamma function — The thermodynamics of the (classical or quantum) truncated Boltzmann distribution involve the normalized lower incomplete Gamma function $P(a, z)$, defined as [S3]:

$$P(a, z) = \frac{\gamma(a, z)}{\Gamma(a)} = \frac{1}{\Gamma(a)} \int_0^a dt e^{-t} t^{z-1}. \quad (\text{S1})$$

For given values of the trap size L and atom number N , the classical partition function Z^{cl} is proportional to $P(N, \beta E_M)/\beta^N$. Hence, a is of the order of N , whereas $z = \beta E_M$ is the ratio of the threshold energy to the temperature. For a given a , the function $P(a, z)$ resembles a step function (see Fig. S3(a)) which is equal to 0 for

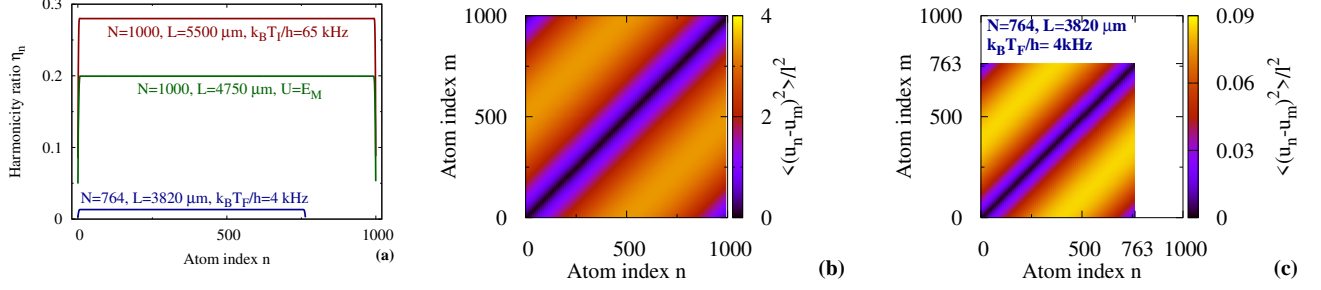


FIG. S1. (a) Harmonicity ratio η_n for the long chain (Fig. 5 in the main text), at the beginning of the evaporation (red), just before the first expulsion (green), and at the end of the evaporation (blue). (b) and (c): Spatial correlator $\langle (u_n - u_m)^2 \rangle / l^2$ at the beginning ((b), $N = 1000, L = 5500 \mu\text{m}$) and the end ((c), $N = 764, L = 3820 \mu\text{m}$) of the evaporation, in units of $l = L/N$.

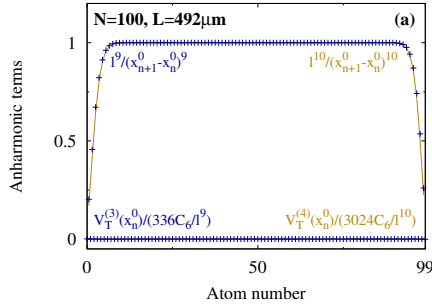


FIG. S2. Third- (blue crosses) and fourth-order (golden lines) anharmonic amplitudes from the interaction energy (non-zero amplitudes) and the trapping potential (negligible amplitudes), calculated for the shorter chain of Fig. 3 in the main text, just before the first expulsion. They are expressed in units of their bulk values, namely $56C_6/l^9$ and $126C_6/l^{10}$.

small z (representing the truncation for large T) and to 1 for large z (truncation plays no role for small T). The smooth transition occurs for $z \approx a$, so that truncation plays a role for $k_B T / E_M \gtrsim 1/a$. The parameter $a = 3$ for a gas in a truncated 3D harmonic trap [S4], whereas for Rydberg chains $a \approx N$ ranges from 40 to 1000. Hence, Rydberg chains are affected by the truncation starting from much lower temperatures than gases are.

Quantum partition function — For a given L , and assuming $E_M^{\text{quant}} \gg E_{ZP} + \hbar\omega_N$, we evaluate the quantum partition function Z^{quant} for $k_B T \gtrsim E_M^{\text{quant}} / N$ using Eq. 2 in the main text, replacing E_M^{cl} by E_M^{quant} . We go beyond the quasiclassical integral expression and include the leading-order quantum correction, proportional to \hbar^2 [S5, §33]. Hence, we write $Z^{\text{quant}} = Z^{\text{cl}}(1 + \langle \hbar^2 \chi_2 \rangle)$, where the correction $\langle \hbar^2 \chi_2 \rangle$ is expressed in terms of the

moments $\langle x_k^2 \rangle_{\text{cl}}$, $\langle p_k^2 \rangle_{\text{cl}}$ and $\langle x_k^2 p_k^2 \rangle_{\text{cl}}$ of Z_{cl} . We find:

$$\langle \hbar^2 \chi_2 \rangle = E_M^2 / \sum_{k=1}^N (\hbar\omega_k)^2 = \frac{z^2}{24} \left(-1 + [3z - 5(N+1)] \frac{z^N e^{-z}}{\Gamma(N+2) P(N, z)} \right), \quad (\text{S2})$$

with $z = \beta E_M$. For $k_B T < E_M / N$, we use the quantum partition function $Z_0 = \prod_{k=1}^N [\text{csch}(\beta\hbar\omega_k/2)/2]$ of a non-truncated chain. The functions U^{quant} and S^{quant} overlap with those extracted from Z_0 for a range of values of $k_B T$, thus yielding the full quantum thermodynamic functions. The classical and quantum predictions for U and S are compared on Fig. S3. At the beginning of the evaporation (panel (b)), they only differ over a narrow range of temperatures near $T = 0$; the difference is more striking near the end of the evaporation (panel (c)).

Numerical evaluation — The evaluation of $U(L, T)$ and $S(L, T)$ involves calculating $P(a, z)$ for $40 \leq a \leq 1000$. In order to capture the steep variation of these functions for $z \sim a$, we resort to arbitrary-precision numerics using the Boost.Multiprecision C++ library [S6].

CONSTANT ATOM NUMBER PLATEAUX

Between two atomic expulsions, the chain undergoes an adiabatic compression during which N remains constant (see Fig. 3 in the main text). For $k_B T_I / h \sim 65 \text{ kHz}$, these constant- N plateaux are smoothed out for most of the evaporation because of the uncertainty $\Delta U_I = U_I / \sqrt{N_I}$ on the initial energy. Indeed, it reflects on the entropy as $\Delta S_I = \Delta U_I / T_I$, and leads to sizable fluctuations $\Delta S^{(N)}$ during most of the evaporation. These yield the uncertainty $\Delta L_f^{(N)} = \Delta S^{(N)} / S_{\text{max}}^{(N)'}(L_f)$ on the trap size $L_f^{(N)}$ at which the atom N is expelled.

For shorter chains, the constant- N plateaux become well resolved at the end of the evaporation, as the chain approaches its ground state. For Fig. 4 in the main

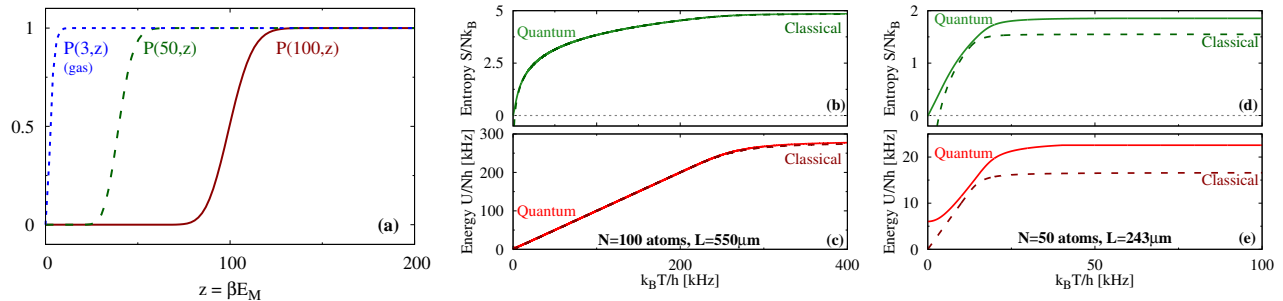


FIG. S3. (a) Normalized incomplete Gamma function $P(a, z)$ as a function of $z = \beta E_M$, for $a = 3, 50$, and 100 . (b) and (c): $s = S/N$ and $u = U/N$ as a function of T for 100 atoms in a trap of size $L = 550 \mu\text{m}$ (beginning of the evaporation on Fig. 3 of the main text). (d) and (e): s and u for 50 atoms with $L = 243 \mu\text{m}$ (close to the end of the evaporation on Fig. 2).

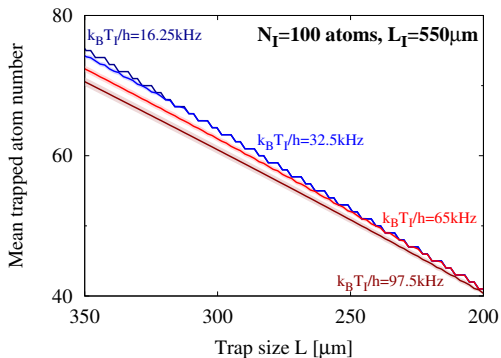


FIG. S4. Mean trapped atom number as a function of the trap size L for the short chain initially comprising $N_I = 100$ atoms with $L_I = 550 \mu\text{m}$ for various initial temperatures. The red curve, calculated for $k_B T_I = 65 \text{kHz}$, corresponds to Fig. 4 of the main text. The discrete steps on the atom number become visible at the end of the evaporation; for lower initial temperatures, they are well resolved earlier on. The shaded areas show the mean standard deviation due to the initial fluctuations $\Delta U_I = U_I/\sqrt{N_I}$ on the quadratic energy.

text and $k_B T_I/h = 65 \text{kHz}$, these plateaux are visible when the remaining trapped atom number $N \lesssim 45$ (see Fig. S4), in agreement with the classical-dynamics results of Ref. [S2]. The plateaux are resolved earlier on for lower initial temperatures and later on for higher ones.

QUASI-UNIVERSALITY

We now focus on longer chains with $N \sim 1000$ and $l \sim 5 \mu\text{m}$. Then, the quadratic energy $U(N, L, T) = Nu(l, T)$, the entropy $S(N, L, T) = Ns(l, T)$, their maxima $U_{\text{max}}(N, L) = Nu_{\text{max}}(l)$ and $S_{\text{max}}(N, L) = Ns_{\text{max}}(l)$, and the zero-point energy $E_{\text{ZP}}(N, l) = Ne_{\text{ZP}}(l)$, are all extensive.

Energy and entropy — We consider two consecutive adiabatic plateaux corresponding to N and $N-1$ trapped atoms. Equation 5 in the main text provides the initial

energy per particle $u_i^{(N-1)} = U_i^{(N-1)}/(N-1)$ for the second plateau in terms of its final value for the first one, $u_f^{(N)} = U_f^{(N)}/N$, and the mean distance $l_f^{(N)} = L_f^{(N)}/N$:

$$u_i^{(N-1)} = u_f^{(N)} + (u_f^{(N)} + 7C_6/l_f^{(N)6} - V_L)/N. \quad (\text{S3})$$

Hence, starting from the first atomic expulsion, u remains close to the universal curve $u = u_{\text{max}}(l)$, within small deviations which decrease like $1/N$. Furthermore, the entropies $s^{(N)} = s_{\text{max}}(l_f^{(N)})$, which are constant during each plateau, all lie near the universal curve $s = s_{\text{max}}(l)$. Both of these properties are illustrated on Fig. 5 of the main text for various $u_I = U_I/N_I$, which set the mean atomic distance l_1 at which the first expulsion occurs.

Fluctuations — The quasi-universality of the evaporation constrains the fluctuations Δu and Δs on the energy and entropy per particle to follow those on the atomic distance, Δl . Neglecting the small deviations from the universal curves $u = u_{\text{max}}(l)$ and $s = s_{\text{max}}(l)$, they satisfy $\Delta u/\Delta l = u'_{\text{max}}(l)$ and $\Delta s/\Delta l = s'_{\text{max}}(l)$ (see Fig. S5).

The constraint on $\Delta u/\Delta l$ has an important consequence. As l decreases, $u_{\text{max}}(l)$ tends towards $e_{\text{ZP}}(l)$ (see Fig. 5(b) in the main text). Hence, the derivative $u'_{\text{max}}(l)$ goes to zero. The fluctuations Δu do not vanish, therefore Δl increases and so does $\Delta n = (n/l)\Delta l$ (see Fig. S5(a)). Thus, as long as the quasi-universal regime holds, the constant- N plateaux will be poorly resolved. If the evaporation proceeds further, it will eventually drive the system out of the universal regime. Then, we expect to recover the short-chain behavior described in Sec. . For the chain considered in Fig. S5, this occurs beyond the validity range of our assumption $E_M^{\text{quant}} \gg E_{\text{ZP}} + \hbar\omega_N$, and will be investigated elsewhere.

Non-universality of N/N_I — The entropy per particle $s(l, u)$ may be seen as a function of l and u . The derivative $\partial s/\partial u|_l = 1/T$ goes to zero on the curve $u = u_{\text{max}}(l)$, which is reached for $T \rightarrow \infty$. However, our numerical results show that $\partial s/\partial l|_u$ diverges along the curve $u = u_{\text{max}}(l)$ (see Fig. S6). Therefore, $s(l, u)$ may not be linearized near this curve, and the entropy difference

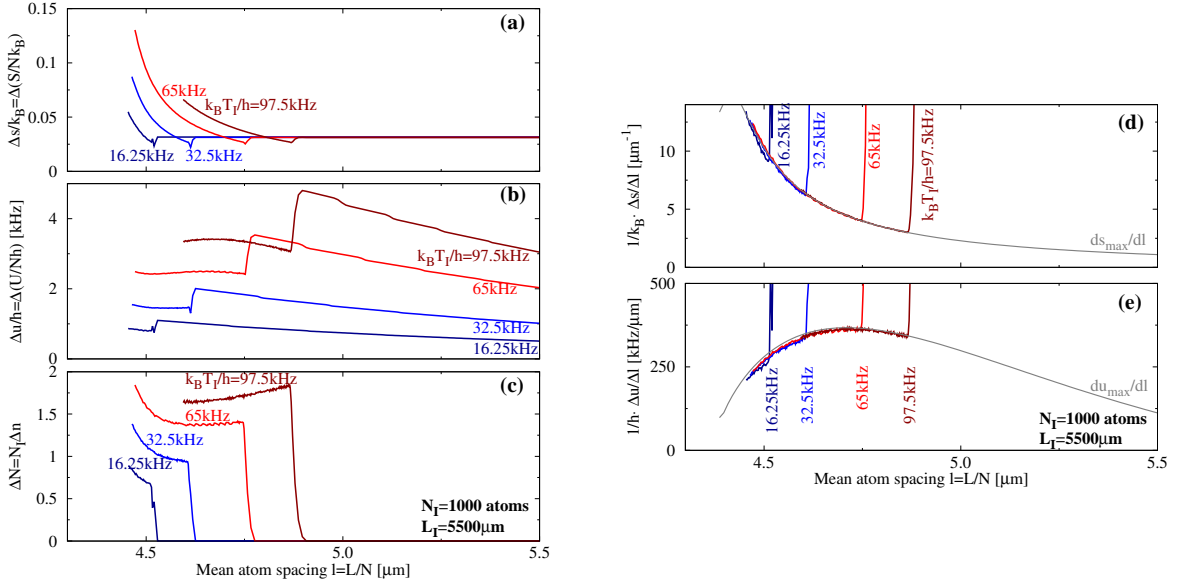


FIG. S5. Standard deviations (a) Δs , (b) Δu , and (c) Δn on the entropy per particle $s = S/N$, the energy per particle $u = U/N$, and the remaining atom fraction $n = N/N_I$, for the long chain of Fig. 5 in the main text. The ratios (d) $\Delta s/\Delta l$ and (e) $\Delta u/\Delta l$, with $\Delta l = (l/n)\Delta n$, closely follow the derivatives ds_{\max}/dl and du_{\max}/dl starting from the first expulsion.

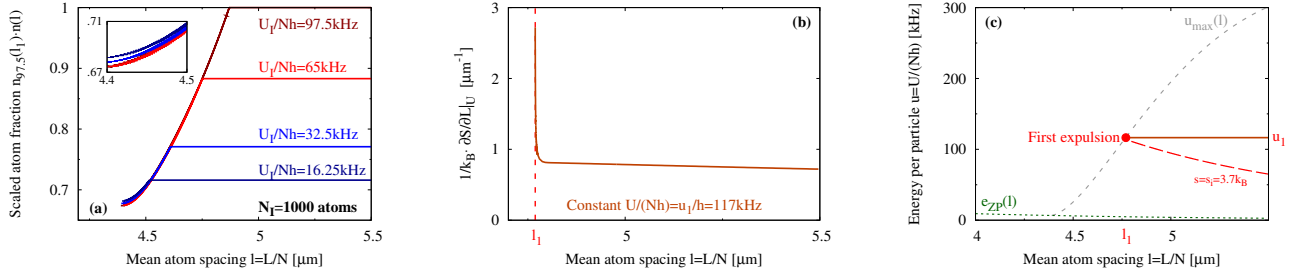


FIG. S6. (a) Scaled atom fraction $n = N/N_I$ for $N_I = 1000$ and various u_I , showing an approximate scaling whose breakdown is visible in the inset. (b) The derivative $\partial s/\partial l|_u$ calculated along the horizontal dark red path on panel (c). This path crosses the curve $u = u_{\max}(l)$ (dashed gray line) at the first expulsion point (l_1, u_1) for $u_I/h = 65$ kHz. The dotted-dashed red line shows the isentropic curve followed up to the first expulsion.

$s^{(N-1)} - s^{(N)} = s(l_i^{(N-1)}, u_i^{(N-1)}) - s(l_f^{(N)}, u_f^{(N)})$ goes to zero slower than $1/N$. This rules out any exact universal behavior for the atom number fraction $n = N/N_I$. However, the deviation from universality is small. For a given N_I , we consider two initial energies $u_{I1} < u_{I2}$, and compare the curves $n_{u_{I1}}(l)$ and $n_{u_{I2}}(l)$ for $l < l_1$, where l_1 is the mean atom spacing leading to the first expulsion for u_{I1} . Our numerical results show that these two curves nearly satisfy the scaling relation which would have been exact had $\partial s/\partial l|_u$ not been divergent, namely $n_{u_{I2}}(l_1)n_{u_{I1}}(l) \approx n_{u_{I2}}(l)$ (see Fig. S6(a), whose inset highlights the breakdown of this scaling behavior).

The divergence of $\partial s/\partial l|_u = p/T$ along the curve $u = u_{\max}(l)$ signals that the pressure p goes to infinity faster than T does. This starkly contrasts with the behavior of the ideal gas, where $p/T = nk_B$ is finite, its constant

value being set by the particle density n .

- [S1] N. D. Mermin, Phys. Rev. **176**, 250 (1968).
- [S2] T. L. Nguyen, J. M. Raimond, C. Sayrin, R. Cortinas, T. Cantat-Moltrecht, F. Assemat, I. Dotsenko, S. Gleyzes, S. Haroche, G. Roux, T. Jolicoeur, and M. Brune, Phys. Rev. X **8**, 011032 (2018).
- [S3] DLMF, “NIST Digital Library of Mathematical Functions,” <http://dlmf.nist.gov/> (2018).
- [S4] O. J. Luiten, M. W. Reynolds, and J. T. M. Walraven, Phys. Rev. A **53**, 381 (1996).
- [S5] L. D. Landau and E. M. Lifshitz, *Statistical Physics, part 1*, 3rd ed. (Elsevier, 1980).
- [S6] “Boost.Multiprecision library,” https://www.boost.org/doc/libs/1_70_0/libs/multiprecision/doc/html/index.html (2019).